

Single-column model and large eddy simulation of the evening transition in the planetary boundary layer

G. C. Cuchiara¹ · B. Rappenglück¹

Received: 28 March 2016 / Accepted: 22 February 2017 / Published online: 27 February 2017
© Springer Science+Business Media Dordrecht 2017

Abstract In the present study, the well-known case of day 33 of the Wangara experiment is resimulated using the Weather Research and Forecasting (WRF) model in an idealized single-column mode to assess the performance of a frequently used planetary boundary layer (PBL) scheme, the Yonsei University PBL scheme. These results are compared with two large eddy simulations for the same case study imposing different surface fluxes: one using previous surface fluxes calculated for the Wangara experiment and a second one using output from the WRF model. Finally, an alternative set of eddy diffusivity equations was tested to represent the transition characteristics of a sunset period, which led to a gradual decrease of the eddy diffusivity, and replaces the instantaneous collapse of traditional diagnostics for eddy diffusivities. More appreciable changes were observed in air temperature and wind speed (up to 0.5 K, and 0.6 m s⁻¹, respectively), whereas the changes in specific humidity were modest (up to 0.003 g kg⁻¹). Although the representation of the convective decay in the standard parameterization did not show noticeable improvements in the simulation of state variables for the selected Wangara case study day, small changes in the eddy diffusivity over consecutive hours throughout the night can impact the simulation of distribution of trace gases in air quality models. So, this work points out the relevance of simulating the turbulent decay during sunset, which could help air quality forecast models to better represent the distribution of pollutants storage in the residual layer during the entire night.

Keywords Planetary boundary layer · Atmospheric modeling · LES · WRF · PBL parameterization

✉ G. C. Cuchiara
gustavo.cuchiara@gmail.com

¹ Department of Earth and Atmospheric Science, University of Houston, 4800 Calhoun Rd, Houston, TX 77204-5007, USA

1 Introduction

The atmospheric boundary layer over land surface displays a well pronounced diurnal cycle. During daytime, surface heating generates positive sensible heat flux from the surface, resulting in an unstable and well-mixed convective boundary layer (CBL). Shortly before sunset radiative cooling of the surface layer results in the development of stable stratification of the planetary boundary layer (PBL). As a consequence a thermally stable boundary layer (SBL) close to the earth's surface evolves. With time, this layer becomes decoupled from the upper portions of the boundary layer (BL) and a residual layer (RL) remains aloft [1]. The mean and turbulent characteristics of the diurnal cycle of the PBL play an important role in determining the transport, storage and dispersion of atmospheric pollutants, especially close to the earth's surface and within the residual layer.

The evening transition, i.e. when daytime PBL turns from a CBL to a SBL, has by far been less studied than the morning transition, and even the definition of the boundary layer during these transitional periods is not well-defined in the literature. Some researchers define it as an instantaneous process, e.g. [2–4], while others treat the transition as a longer process of a few hours [5]. This calls for a more thorough analysis of this time period. Even more, as this transition from the daytime CBL to a nighttime SBL plays an important role in complex atmospheric phenomena such as transport and diffusion of trace constituents. Its processes have been studied since the first decades of the twentieth century, when Taylor [6] reported that strong nocturnal cooling occurs only under weak, non-turbulent winds and hence, turbulent decay at night would not occur if a cloud deck kept the surface warm. A few years later, Richardson [7] made a turbulent kinetic budget analysis and his comparison between the shear production and buoyancy destruction during the early evening transition led him to the derivation of the Richardson index for instability. Mahrt [5] approached the evening transition problem through the result of the Wangara experiment, which was performed in Australia in 1967 and focused on the diurnal variation of meteorological variables in fair weather. Grant [3] presented an observational study using a tethered-balloon system which provided data at several height levels on three consecutive evenings in August 1990 at Cardington, England. Additional observation-based analyses were provided by Acevedo and Fitzjarrald [8], who obtained some observational characteristics of the transition period using a dense network of automated weather stations in the region of Albany, New York. Acevedo and Fitzjarrald noticed that in fair weather with clear skies, the specific humidity increases, and the surface temperature drops, accompanied by an abrupt decay in wind velocity. This relatively high variability of state variables during the first few hours after sunset can be considered as a definition of the evening transition. Grimsdell and Angevine [9] used wind profiler reflectivity and Doppler spectral width data to characterize the evening transition in Illinois. Brazel et al. [10] used observational data obtained from surface weather stations in Phoenix, Arizona to investigate the time lag in the evening transition after local sun down and the flow characteristics of a topographically complex region. Edwards et al. [11] studied the evening transition using observations at Cardington, England, and applying large-eddy simulation (LES) and single-column modeling (SCM). In their work Edwards et al. pointed out the importance of considering synoptic and mesoscale conditions to obtain a reasonable agreement between observations and numerical weather prediction (NWP), when using the SCM mode. Also, Edwards et al. [11] suggested a more rapid decay of the diffusivities with height for PBL parameterizations. Recently, the work performed by Sastre et al. [12] tested the ability of three PBL parameterizations (Mellor–Yamada–Janjic Scheme [MYJ],

Quasi-normal Scale Elimination Scheme [QNSE], and Mellor–Yamada Nakanishi Niino [MYNN]) of the Weather Research and Forecasting Advanced Research (WRF-ARW) to reproduce the evening transition, and identified three types of transitions depending on the intensity of Turbulent Kinetic Energy (TKE).

Over the past decades, a better understanding of some of the complex PBL phenomena has been achieved using LES as a tool to explore different regimes of the boundary layer by generating high-resolution four-dimensional turbulence data. For instance, the representation of moderately stable regimes using LES was often considered a challenge, but is now reasonably well represented [11, 13, 14]. Based on LES results modifications such as explicit treatment of the entrainment process, vertically varying Prandtl number and mixed-layer velocity scale, and non-local mixing (e.g. Noh et al. [15]) have eventually been implemented into the widely used K-profile PBL parameterization [16].

Without the interference of the atmospheric three-dimensional dynamics, SCMs are useful tools to evaluate parameterization schemes and problems related to the representation of physical processes (e.g., cumulus parameterization, land surface interaction, turbulence in PBL, etc.) in NWP models. Recently SCM studies have been carried out to analyze the PBL with respect to different stability regimes. Sharan and Gopalakrishnan [17] compared five closure schemes, including local and non-local closures, using the Cabauw (Netherlands) and EPRI-Kincaid site (United States) observations. They highlighted that the mesoscale model diffusion problem under SBL conditions can be better treated using the classification based on wind intensities than the widely used weakly, moderately, and strongly SBL classification. Cuxart et al. [18] found a large scatter of parameterization results of the stably stratified atmospheric boundary layer in a model intercomparison study. Edwards et al. [11] used a SCM to simulate the evolution of the PBL through the evening transition and the early hours of the night in Carlington (United Kingdom). They emphasized the importance of the synoptic situation when using a SCM in the context of numerical weather forecast. Steeneveld et al. [19] analyzed the prediction of the SBL over land surface for three contrasting nights in CASES-99. They found that the vertical structure, the surface fluxes (apart from its intermittent character) and the surface temperature in the SBL can be modeled for a broad stability range. Mauritsen et al. [20] presented numerous large-eddy simulations, including a wide range of neutral and stably stratified cases to formulate a turbulence closure for neutral and stratified atmospheric conditions. Baas et al. [21] formulated a methodology to compare a SCM with observed low level jets using the European Centre for Medium-Range Weather Forecast (ECMWF) model. Kumar et al. [22] investigated the impact of surface flux formulations and geostrophic forcing in the diurnal cycle of the PBL using LES. More recently, Bosveld et al. [23] performed a SCM intercomparison using the Cabauw observatory archive, and focused on the diurnal cycle of PBL models. All of the studies mentioned above guided improvements for PBL parameterizations, not only using simplified forcings but also complex realistic forcings, which facilitate the comparison with the observation.

In summary, open questions remain about the dynamic and turbulence structure of the evening transition. The goal of this work is to provide an integrated approach combining observational data with supplementary information provided from LES to assess the performance of the WRF model in simulating the PBL evening transition. To address this objective, firstly the sensitivity of a non-local closure, widely used PBL scheme (Yonsei University—YSU) was evaluated for the clear sky condition of day 33 of the Wangara case study. Because LES provides properties of the flow which are not visible in observed data, the LES model is a helpful tool to represent characteristics of the boundary layer in the PBL parameterization. Likewise SCM helps to point out potential common biases of the

model that are hard to capture with a full general circulation model. Lastly, we tested an alternative set of eddy diffusivity equations, proposed by Carvalho et al. [24], added to the WRF Yonsei University (YSU) PBL scheme to better represent the shear dominated SBL (near the ground) and the convective decay elevated turbulence (aloft) during the evening transition. We discuss how the model results using the YSU PBL scheme compare to the LES model, and to the alternative parameterization.

This paper is organized as follows. The description of the SCM and LES using WRF and the methodology used in this work for the two distinct model configurations are described in section two. We discuss the different surface representations in the experiment in Sect. 2.1. The ability of a widely used PBL scheme in the WRF model to simulate the evening transition period is compared with LES and observations in Sect. 2.2. In Sect. 2.3 a brief description of the alternative set of eddy diffusivity equations added to the YSU PBL scheme along with results is presented. Finally, conclusions are compiled in the last section.

2 Methodology

2.1 The day 33 of Wangara experiment

The Wangara boundary layer experiment [25] took place at a large flat and vegetation-free site near Hay, Australia ($34^{\circ}30'S$, $144^{\circ}56'W$) from 15 July to 27 August 1967. The meteorological observations included vertical profiles of wind, temperature, and mixing ratio; surface geostrophic, and surface to 2 km thermal winds; and micrometeorological profile measurements. The radiosondes collected potential temperature and wind data every 50 m from the surface up to 1 km (km) above ground level (agl), and every 100 m above 1 km up to 2 km agl. Observational data of days 33–35 of the experiment have been commonly used to study important process within the PBL, and to evaluate one-dimensional PBL numerical prediction models [5, 26–28]. In our study, the results from SCM and LES are analyzed for 1 day, August 16, the so called day 33 of this experiment. This period was characterized by cloudless skies, very little horizontal advection of heat and moisture, and no influence of synoptic frontal influence within 1000 km. The region was under an influence of a high-pressure system (1034 hPa) centered over the Wangara experimental site that slowly moved southeast of the region by the end of the day 33 and beginning of day 34. Furthermore, the daytime PBL was highly convective and capped at approximately 1000 meters (m) agl by a well-defined stable layer. The sunrise was at 07:12 local time (LT) and the sunset was at 17:45 LT. Hence, these conditions satisfy the one-dimensional PBL model assumptions, which include stationary synoptic situation, clear skies and the absence of fog. All results focused on the evening transition of the day 33 between 9 LT and 21 LT.

2.2 Sensitivity analysis using single-column modeling (SCM)

The WRF model is a weather prediction system designed to serve for both atmospheric research and operational forecasting needs (www.wrf-model.org). WRF is being used to study atmospheric dynamics and land–atmosphere interaction at various scales. The WRF physics options comprise several categories, each containing several choices. The physics categories include microphysics, cumulus parameterization, PBL, land-surface model, and

radiation. Thus, the WRF model is suitable to study the phenomena in the Earth’s atmosphere at a wide variety of scales.

The SCM is the single-column version of the WRF (WRF-SCM) model. WRF-SCM is a one-dimensional stand-alone implementation of the standard WRF-ARW release [29, 30]. Solving the same conservation equations for mass, momentum, energy, and moisture in the atmosphere, the WRF-SCM runs on a 3×3 stencil with periodic lateral boundary conditions in x and y . The WRF-SCM experiments have been configured as follows. The simulations are initialized at 09 LT, August 16, 1967 and the integration time is 12 h. The observed vertical profile of potential temperature, u and v component of the wind, and water vapor mixing ratio were used as initial condition (Fig. 1). The full dynamical evolution of the synoptic conditions cannot be represented in SCM simulation. One common strategy used in this work is to specify the geostrophic wind (Fig. 1). As highlighted by Bosveld et al. [23] the geostrophic wind is an important variable that affect the structure of SBL. The observational data available for the Wangara experiment are not sufficient to initialize the SCM, because it is limited to the heights below 2 km agl. Thus, we needed to prescribe the initial profiles using observations up to 2 km agl [25] and adding output from the WRF forecasting model for layers aloft. Note that we compared observations up to 2 km agl with the WRF output for consistency (not shown), and based on the reasonable agreement we did not perform any additional adjustment.

According to the information provided by Clarke et al. [25] the area of the Wangara experiment was a flat land covered predominantly by very sparse grass, with occasional patches of low shrubs. Thus, the land use and soil properties data used in this SCM simulation was chosen based on Clarke et al. and previous work by McNider and Pielke [31]. The surface properties were based on the United States Geological Survey (USGS—33 categories) that provided values for parameters like roughness, emissivity, albedo, etc. Also described by Clarke, all terrain heights are equal and set to 92.8 m above sea level (asl).

Usually, in standard forecast simulations the number of vertical grid level of range from 20 to 40 vertical grids up to ~ 12 km agl, with 10–15 levels within the first 2 km agl. For this study we decided to use a highly resolved vertical grid of 80 levels up to the total model height of 12 km agl. The WRF model levels follow the terrain, and the lowest model levels near the ground are located approximately at 28, 57, 86, 117, and 148 m agl. The time step is 10 min. An idealized simulation (i.e. no consideration of full dynamical evolution of the synoptic situation) was configured to investigate the ability of a non-local

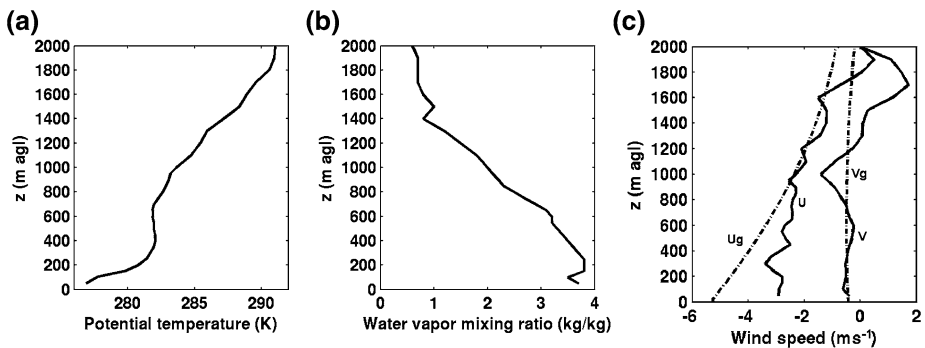


Fig. 1 Initial mean condition for Wangara: **a** potential temperature, **b** water vapor mixing ratio, and **c** u – v component and geostrophic wind

closure PBL scheme (Yonsei University—YSU) to represent the evening transition of day 33 of the Wangara experiment. This PBL scheme was chosen because it is a well-documented and widely used PBL scheme for both NWP and air quality models (AQM). The physics parameterization for the experiment includes the WRF Single Moment 3-class scheme microphysics [32], the rapid radiative transfer model (RRTM) long wave radiation [33], the Dudhia shortwave radiation scheme [34], the unified Noah land-surface model (LSM) [35], and the Pennsylvania State University/National Center for Atmospheric Research mesoscale model (MM5) similarity scheme surface layer model [36–39]. The characteristics of the SCM are listed in Table 1.

2.3 The large eddy simulation (LES)

The WRF–LES is a tool to study turbulent flows within the PBL. The Advanced Research WRF (ARW) model solves fully compressible equations on a mass coordinate and uses finite differences in horizontal and vertical directions. Moeng et al. [40] compared results from the WRF model framework, which included the basic Runge–Kutta scheme for LES of boundary layer turbulence, to field measurements (e.g., [41]), laboratory data (e.g., [42]), and previous LES studies (e.g., [43–46]). Our study uses the LES model and statistics package of the Advanced Research WRF model, version 3.6 (see [47] for a detailed description). This statistics package is based on the System for Atmospheric Modeling (SAM) algorithm [48]. All LES results shown in this work are horizontal mean statistics saved every simulated minute, without time averaging, while the full three-dimensional snapshot is saved every fifteen simulated minutes. The surface-layer physics is described by the Monin–Obukhov scheme [49] with a Carlson–Boland viscous sub-layer and standard similarity functions following Paulson [36] and Dyer and Hicks [37]. The mixing terms option is evaluated in physical space (i.e. describing the diffusion using the velocity stress tensor in x , y , and z directions) and the turbulence parameterization is the Smagorinsky first order 3D closure.

The simulation is run with a horizontal grid spacing of 40 m and a vertical grid spacing of 15.625 m. The domain has 128 (x) \times 128 (y) \times 128 (z) grid points and is periodic in both the x and y directions. The top of the domain is set at 2 km agl, which is two times above PBL top on that specific day 33 of the Wangara experiment. The model runs for a 12 h period starting at 9 LT and with time step of 0.5 s. Previous work by Yamada and Mellor [26], André et al. [27], and Musson-Genon [28] took into account longwave

Table 1 Parameters in the WRF-SCM Wangara experiment simulation

Simulation time	16 August 1967—09 LT
Geographic coordinate	34.5°S; 144.93°E
Coriolis parameter	$-0.82 \times 10^{-4} \text{ s}^{-1}$
Total column height	12 km
Time step	60 s
Vegetation fraction	0.14
Land use index	Mixed shrubland/grassland
Soil type	Loam
Surface albedo	0.22
Emissivity	0.93
Roughness length	0.01 m
Terrain height	92.8 m

radiation cooling. However, since the simulations showed little sensitivity to this inclusion, no radiative effects are included in the LES run. Instead a Rayleigh relaxation layer was added near the top of the model to control reflection from the upper boundary [30].

A critical question concerns the surface fluxes initialization, and this can be a source of uncertainty. Most of the Wangara atmospheric boundary layer modeling studies (e.g., [50–53]) chose to prescribe the surface heat fluxes instead of predicting or diagnosing them. Typically, a sine function with a half period of 11 h and peak values of 0.216 K m s^{-1} at 13 LT were assumed for prescribing sensible heat fluxes. The Wangara micrometeorology data was extensively analyzed by Hicks [54]. According to Hicks [54] the surface-layer similarity theory of wind speed differences and temperature from 1 to 4 m agl were used to derive the sensible heat flux (SHF). The latent heat flux (LHF) was parameterized by Hicks [54] as $\text{LHF} = 1.3 \times 10^{-4} \times \text{SHF}$. In the approach used by Hicks [54] the surface fluxes were estimated for the larger area of the Wangara experiment rather than just for the smoother central site. The Wangara experiment location was chosen to be uniform in roughness [25]. However, according to Hicks [54] the central site was quite bare compared with its surrounding, and the roughness was considered by Hicks to be 1.2 mm. For this reason, we performed two LES using different surface forcings: one using the fluxes calculated by the Hicks’ method [54], and the other using the output from the WRF model for direct comparison with the YSU PBL scheme (hereinafter LES-HM and LES-YSU, respectively). This experiment can potentially magnify the difference between the observation and simulation. These differences will be further explored in the next section.

Although relevant process such as the dynamic or the surface forcings are prescribed in this experiment, both SCM and LES simulations were considered idealized. The synoptic situation in SCM and LES was represented by geostrophic winds only. While other important process like temporal variations of the mesoscale forcing, for instance, are not addressed in these simulations, the strength of this approach is the possibility to analyze differences in mixing efficiency, and to examine the behaviour of turbulence parameters as well as the characteristics of heat fluxes and eddy diffusivities provided by PBL parameterization.

3 Results and discussion

3.1 Surface fluxes

The surface parameters such as friction velocity, sensible, and latent heat flux imposed to LES according to Hick’s method (HM) [54], and calculated by Noah-LSM for the SCM

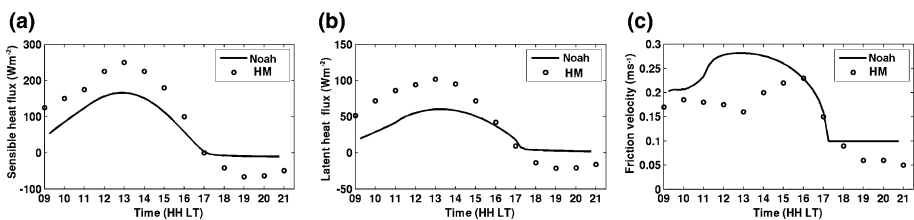


Fig. 2 Surface variables according to HM (dots) and calculated by Noah-LSM (line) for a sensible heat flux, b latent heat flux, and c friction velocity

simulation are shown in Fig. 2. Overall, there are differences in the calculation of the surface fluxes in all three variables. The sensible heat flux (Fig. 2a) presents a period of intense cooling 1 h after the diurnal maximum (13 LT) until the sunset. Although both Noah-LSM and HM agreed in the point of time when the flux reaches 0 W m^{-2} , the sensible heat flux calculated according to HM shows a continuing strong cooling after reaching the zero value. This feature can be the reason for the fact that the LES simulation using this initialization presented a very cold SBL. Regarding the surface energy balance the latent heat flux is another important variable and is presented in Fig. 2b. During the daytime the latent heat flux calculated by the LSM shows a difference of 10 W m^{-2} . The surface friction velocity, u^* (Fig. 2c) presents different values during the evening transition and afterwards. The lower values for sensible and latent heat flux calculated by Noah compared with HM before 21 LT (maximum deviation up to 80 and 50 W m^{-2} , respectively) result in less strong fluxes from the surface and consequently up to 0.1 m s^{-1} higher friction velocity. Also, the lower values of the surface fluxes are due to the land cover provided by USGS used in the Noah LSM calculation. This is in agreement what was mentioned before, i.e. the HM surface estimations represent the larger area of the Wangara experiment rather than just the central site which was applied in the Noah approach. The friction velocity and heat fluxes have direct impact on 10 m wind speed diagnosed by WRF, which will be discussed in the last section.

3.2 Comparison of the YSU PBL scheme and LES

Figure 3 presents the observed evolution of mean potential temperature and PBL height observed in the Wangara experiment and calculated by the YSU PBL scheme. The variations among the model simulation results of the daytime CBL will have an influence on the simulation of the subsequent transition to nighttime simulation. A thin, very

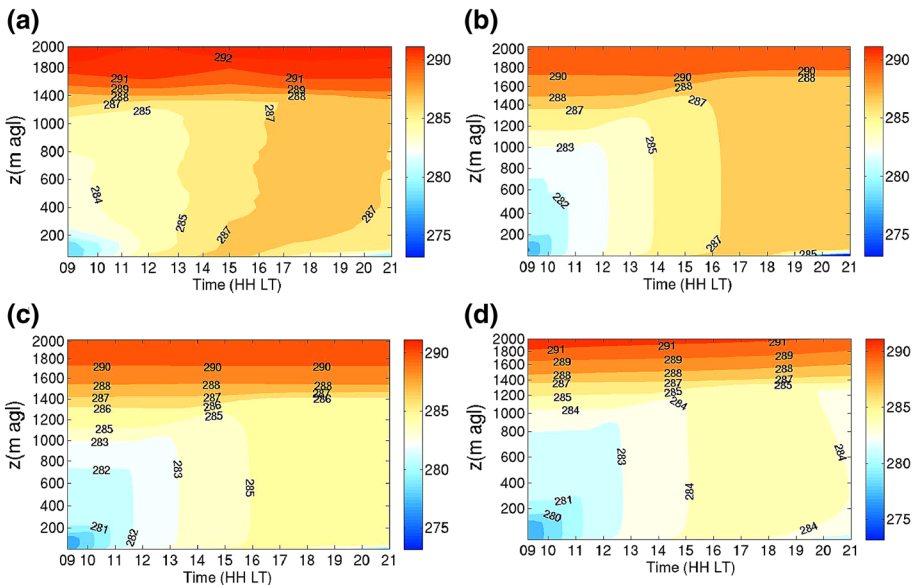


Fig. 3 Spatial and temporal distribution of potential temperature (K) for **a** observation, **b** LES-HM, **c** LES-YSU, and **d** YSU for Wangara day 33

unstable surface layer below 200 m agl, and a mixed layer topped by a stable inversion layer (at approximately 1000 m agl) are observed during daytime. This feature can be expected and is qualitatively well reproduced by LES-HM, LES-YSU, and YSU. However, there are few discrepancies between simulated results and observations. Compared with the observations all the three model simulations present a cold bias for potential temperature with LES-HM having the least bias among the simulations. Similarly, Basu et al. [55] and Yamada and Mellor [26] reported simulated mixed layer temperatures lower than observations during daytime in their LES simulations. This cold bias is most evident at 12 LT, when this bias reached ~ 2 and ~ 3 Kelvin (K), for LES-HM and LES-YSU respectively. The YSU scheme displays slight (~ 1 K) cooler PBL potential temperature when compared with the LES-YSU. At 15 and 18 LT, the LES-HM captures the temperature relatively better within PBL. For the observation and model outputs (also previous works), a subjective way to estimate the PBL height based on Rappenglück et al. [56] was used in this work. The PBL heights (sharp increase in potential temperature) estimated from observation were 1000, 1200, 1300 m agl at 12, 15, and 18 LT, respectively. We estimate the uncertainty of the PBL height to be on the order of ± 50 m. The YSU scheme overestimated the PBL height by 100 m at 12, 15, and 18 LT. The LES-YSU better represented the PBL height which agreed quite well with the estimations (1000, 1200, and 1300 m at 12, 15, and 18 LT). The PBL height was underestimated by ~ 200 m in the works of Yamada and Mellor [26] and overestimated by less than ~ 50 m by André [27].

We defined the evening transition as the time period when the surface heat flux becomes negative and a stably stratified layer starts to develop close to the surface. In our case study this is around 17 LT. Throughout the time of the transition, there is a period of fast cooling below 100 m, but the residual layer above stays at the same temperature. LES-HM, LES-YSU and YSU scheme, capture this feature realistically. During the late evening transition (after 18 LT), a SBL begins to grow from the surface, with observed potential temperature displaying a negative curvature. The model simulations capture this feature reasonably well. The LES-YSU case presents similar temperatures but underestimates the height of the inversion, showing a layer of only a few meters depth close to the ground. The YSU PBL scheme (Fig. 3d) shows a good agreement with LES-YSU, but it is about 1 K colder. In previous works the height of the SBL could not be captured well either. For instance, Basu et al. [55] found shallower SBL depth during nighttime when compared with observations. However, in our case the LES-HM model (Fig. 3b) captures well the height of the inversion, approximately 30 m agl at 21 LT, but shows a strong cold bias. As mentioned by Mahrt [57] the dynamics of the SBL are governed by multiple processes. However, for cases with reasonably geostrophic forcings, no fog formation, and for horizontally homogeneous conditions, the dominant processes are thermal coupling of the surface, turbulent mixing and radiative cooling. A plausible explanation for the LES-HM bias in the SBL thickness is the lack of longwave radiation cooling physics. However, earlier studies [26–28] which took into account longwave radiation cooling were not able to capture the thickness of the Wangara SBL either. The discrepancy between the timing and altitude of SBL growth in the model highlights the need for a better understanding of the evening transition and nocturnal boundary layers (especially the strongly stratified regimes). In our results the temperature and the height of the inversion were directly affected by the thermal coupling of the surface with the adjacent atmospheric layer.

The estimated daytime PBL height (Fig. 4) is defined as the altitude where the minimum sensible heat flux height is observed [11]. During nighttime the PBL height is estimated as the height at which the mean local stress falls to 5% of its surface value multiplied by the factor $1/0.95$ [4]. The PBL determination in the YSU scheme is based on

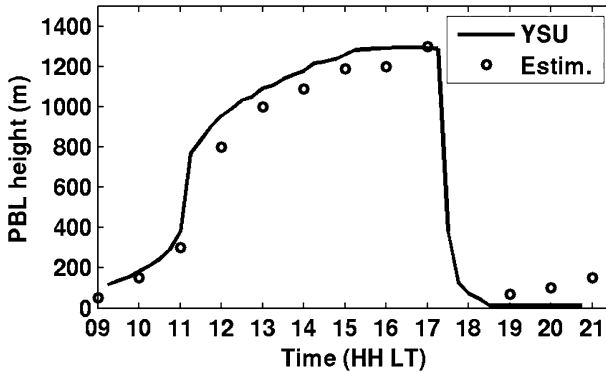


Fig. 4 Calculated PBL height for the YSU scheme (*lines*). The *circles* denote the prescribed PBL height during daytime by Kosovic and Curry [13] and during nighttime by Beare et al. [14]

the bulk Richardson (Ri) number formalism. The critical Ri number is 0.25 under stable conditions and 0 under unstable conditions. At the end of the afternoon, when the surface heat fluxes begin to decrease sharply, and the turbulent kinetic energy begins to decay, the daytime PBL switches from a convective well-mixed layer to a stable nocturnal PBL. The PBL collapses during the transition from a convective unstable to a stable regime. In the YSU scheme this transition happens at 17 LT.

The Wangara experiment was mainly designed to obtain measurements for turbulence fluxes and mean variables, and there is no possibility of directly comparing the results of this work with observed turbulence data such as TKE, for instance. However, the reasonable agreement of the flux model results with previous estimations provides confidence that the WRF-LES simulations of turbulence quantities such as TKE are likely realistic and warrant further turbulence structure analysis. The analysis of the spatial and temporal evolution of TKE within the PBL provides us with a sketch of the turbulence structure during the afternoon, and with a tool to evaluate the calculated PBL height in the SCM model. Figure 5 presents the spatial and temporal evolution of TKE (Fig. 5a, c) and ΔTKE vertical profile 15, 30, and 45 min after sunset at 17:45 LT (Fig. 5b, d). ΔTKE is defined as the difference in TKE between two consecutive outputs of the LES results, for instance the term “+45 min” in Fig. 5b, d would indicate: $\Delta TKE = TKE(45 \text{ min after sunset}) - TKE(30 \text{ min after sunset})$. Though turbulence seems to play a minor role in the evolution of the nocturnal mean structure of the PBL, it is of primary importance for turbulent dispersion and consequently vertical redistribution of contaminants during the PBL transition phase and the subsequent night. Both LES experiments took 1 h to spin-up; starting time was 9 LT. According to Fig. 5a, c the PBL stability conditions, for LES-HM and LES-YSU, respectively, ranged from nearly-neutral at the starting time, became convective after 11:00 LT and returned to stable conditions after 17:00 LT. TKE reached a maximum value of 1.7 and $1.5 \text{ m}^2 \text{ s}^{-2}$ between 14:00–15:00 LT, for LES-HM and LES-YSU, respectively, and then gradually decreased until sunset (17:45 LT) when it approached values close to zero. Figure 5b shows vertical profiles of ΔTKE at 15 min intervals after sunset for the LES-HM experiment. Note that values very close to the surface during the convective time will not be considered, since the WRF LES code still has the long-standing problem of law-of-the-wall deficiency in the surface layer for shear driven PBL [40]. 15 min after sunset, ΔTKE in the upper part of the PBL decreases faster than the bottom part, with differences of approximately 0.13 and $0.05 \text{ m}^2 \text{ s}^{-2}$ respectively. Figure 5d presents similar analysis but

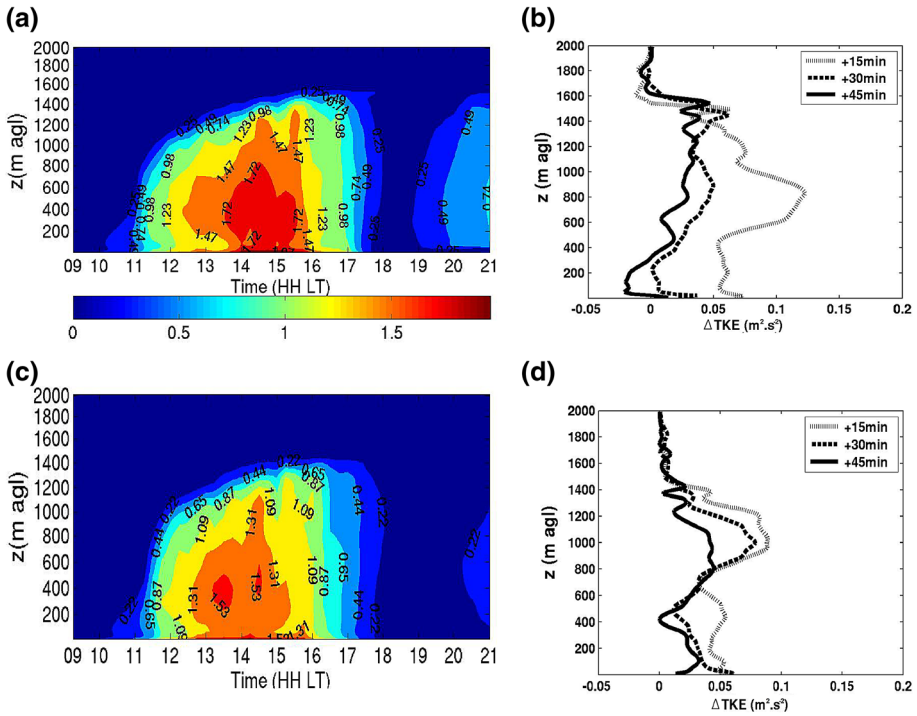


Fig. 5 Spatial temporal evolution of TKE (m^2s^{-2}) for (a, c) the entire LES simulations and for 15, 30 and 45 min time steps (b, d) after sunset (17:45 LT) for LES-HM (top) and LES-YSU (bottom). ΔTKE is defined as the difference in TKE between two consecutive time steps of the LES results

for the WRF-YSU experiment, and the biggest difference between LES-HM and LES-YSU occurs 30 min after sunset: The LES-HM profile 30 min after sunset shows a more uniform TKE decrease (up to $0.05 m^2 s^{-2}$) between 400 and 1400 m, while the LES-YSU profiles at 30 min after sunset indicates a stronger decrease (up to $0.07 m^2 s^{-2}$) between 400 and 1400 m. Although both HM and Noah converge to zero at the same time (17 LT—Fig. 2), it seems that the difference in the intensities of surface fluxes during daytime (HM yields up to $60 W m^{-2}$ more sensible heat flux and up to $50 W m^{-2}$ more latent heat flux than Noah from 09 to 16 LT) and consequently TKE, resulted in variations in the structure of TKE decrease after sunset. The temporal progression in TKE reduction between the upper and bottom part were also analyzed in LES modeling by Darbieu et al. [58] and Rizza et al. [59]. They found that while TKE started to decrease at the top of the PBL, it kept increasing at the bottom of PBL. The results in Darbieu et al. [58] and Rizza et al. [59] are also in agreement with remote sensing observations by Grimsdell and Angevine [9] and Lothon et al. [60], who revealed a decay of TKE dissipation rates from the top to the bottom of the PBL. Shaw and Barnard [61] studied the TKE decay with Direct Numerical Simulation (DNS), based on realistic surface flux decay. They found that turbulence is maintained at the surface relative to upper PBL layers and explained it with the presence of wind shear close to the surface.

The above analysis of the evolution of the turbulence structure during the evening suggests a split of the transition period in two stages. (1) In the early afternoon, from the occurrence of the buoyancy maximum until about 2 h before sunset, the TKE decreases

within the whole PBL, starting first in the upper PBL (earlier decay), while the TKE decrease in the lower part of the PBL occurs half an hour later (later decay). (2) In the late afternoon the TKE decreases more rapidly within the whole PBL than during the early evening transition.

Figure 6a, c present the vertical profile of TKE buoyancy and shear production for around 1 h before and after the sunset for WRF-HM. Figure 6b, d show velocity variances for the same times. At 17 LT the PBL is in a convective regime and at 19 LT in a shear-driven regime. For a convective regime (Fig. 6a, b) the buoyancy production of TKE is predominant and larger close to the ground, because the source of heating is at the surface. Also, the velocity variances are dominated by the large eddies, which have updrafts between 200 and 1000 m and predominantly lateral motions at the bottom and top of PBL (Fig. 6b). On the other hand, when the shear production is dominant (Fig. 6c), the velocity variances are stronger between 100 and 1300 m compared to the surface layer and is dominated by u^2 (Fig. 6d). These figures show that the model was able to capture the transition between buoyancy- to shear-driven PBL regimes.

The rate of the turbulence decay during sunset is a critical parameter for the evening transition. Usually for LES studies the decay is represented in a logarithmic diagram of the TKE integrated over height, and divided by the square of the convective velocity scale w^* at the initial time before the decay. Following previous studies (e.g. [62, 63]) the midday convective timescale is also used to normalize the time. Nieuwstadt and Brost [64] suggested that the temporal evolution during the transition may be investigated using the quantity TKE averaged over the whole PBL. The LES model (Fig. 7) indicated that the turbulent kinetic energy in the decaying mixed layer is in agreement with previous work (e.g. [59, 62, 64]) which indicates that the energy in the PBL decays with a -2 power law function.

Figure 8 presents the spatial and temporal distribution of the wind speed for all simulations and compared to observations. During the convective regime observed wind speeds show a well-mixed boundary layer, with large fluctuations in the wind speed throughout the PBL. During and after the transition this vertical fluctuation of the wind speed is limited, except near the surface where the SBL starts to develop. In the time period between the transition until 21 LT, the wind speed increases rapidly from 4 to 6 m s⁻¹. This increase in wind speed is associated with the formation of a Low-Level Jet (LLJ) during the first hours of day 34 (at 3 LT; not shown), which is beyond the scope of this work. Overall, the SCM underestimated the wind speed during the entire simulation period by 2 m s⁻¹ during the CBL, and by up to 4 m s⁻¹ during and after the transition. The LES simulation showed the best agreement with the observation, but it showed the same

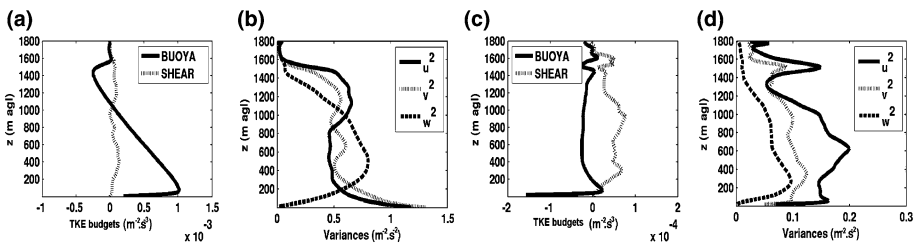


Fig. 6 TKE budgets (buoyancy/shear) production and velocity variances at a, b 17 LT and c, d 19 LT for the LES-HM simulation

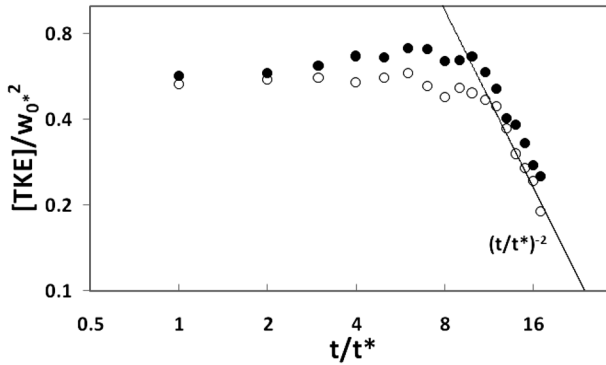


Fig. 7 The volume averaged TKE, scaled by w_0^2 , as a function of the dimensionless time t/t^* for LES simulation. The *continuous line* represents a -2 power law function as a reference in agreement with Nieuwstadt and Brost [64]

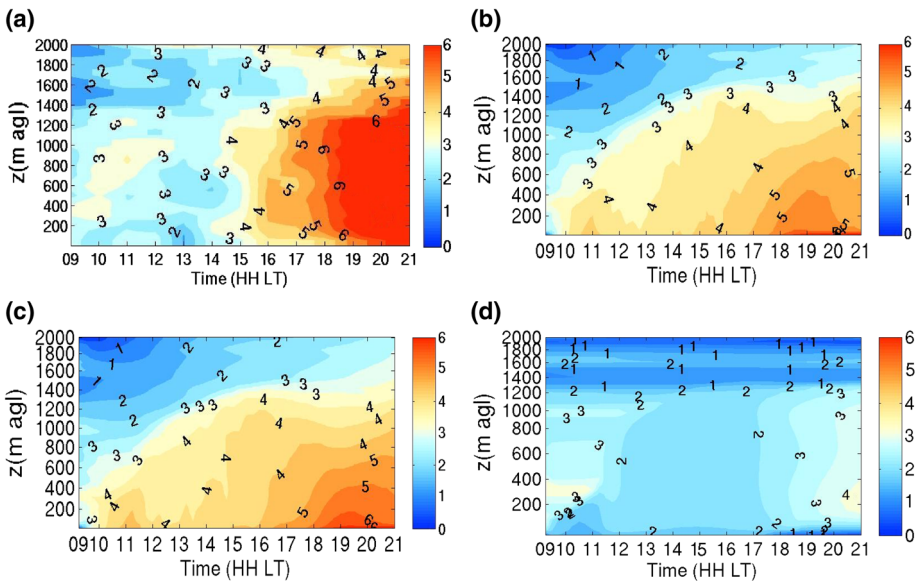


Fig. 8 Spatial and temporal distribution of the wind speed (m s^{-1}) for Wangara day 33: **a** observation, **b** LES-HM, **c** LES-YSU, and **d** YSU

difficulty in representing the wind speed during the transition and the subsequent nighttime PBL.

3.3 Computation of the eddy diffusivities

One of the objectives of this work is to analyze the different mixing characteristic between the standard WRF PBL schemes and alternative eddy diffusivities for the convective decay. Eddy diffusivities are properties of the flow and describe the magnitude of the dispersion. When the grid mesh is bigger than the motions within the PBL, these small-

scale and sub-grid turbulent motions need to be parameterized by a PBL scheme, which properly handles vertical diffusion. The goal of a turbulence parameterization is to predict tendencies (time derivatives) of all prognostic variables (fluid velocity components, temperature, moisture or other advected constituents) at all grid points of a numerical grid due to unresolved turbulent motions [30].

The first-order closure scheme we selected for vertical turbulent transport within the PBL was the YSU [65] PBL scheme. As a popular non-local closure scheme, YSU is based on an earlier medium-range forecast (MRF) scheme, but with a revised vertical diffusion package. The YSU scheme is a non-local first-order scheme in which the vertical transfers are dependent on the bulk characteristics of the PBL and includes counter gradient transports of temperature, momentum arising from large-scale eddies.

The eddy diffusivity coefficient for momentum K_m is formulated as

$$K_m = kw_s z \left(1 - \frac{z}{h}\right)^p \quad (1)$$

where p is the profile shape exponent taken to be 2, k is the von Kármán constant ($=0.4$), z is the height from the surface, and h is the height of PBL. The velocity scale $w_s = u^*/\Phi_m$, where the Φ_m is a non-dimensional profile function implemented in recent versions of WRF (after version 3.4) to accurately simulate the vertical mixing in the nocturnal boundary layer [66, 67].

Figure 9a, b display the temporal and spatial evolution of the eddy diffusivity for momentum K_m in the YSU and, for comparison, simulation results by Yamada and Mellor [26], respectively. As seen in Fig. 9a WRF-SCM was able to reproduce the spatial and temporal variation of K_m . The results obtained by the YSU PBL scheme are in agreement with the results modeled previously by Yamada and Mellor [26]. Both simulations indicate that the turbulence is very active during daytime. The intensities of K_m modeled in the YSU scheme is $10 \text{ m}^2 \text{ s}^{-1}$ higher than those calculated by Yamada and Mellor. Also, the center of maximum turbulence is located at the same level, between 400 and 800 m agl.

3.4 Parameterization of the PBL for the sunset transition period

In turbulent dispersion models, the selection of an adequate PBL parameterization plays a fundamental role to evaluate the pollutants concentration in the lower troposphere. Therefore, the efficiency of each approach to reproduce correctly the pollutants

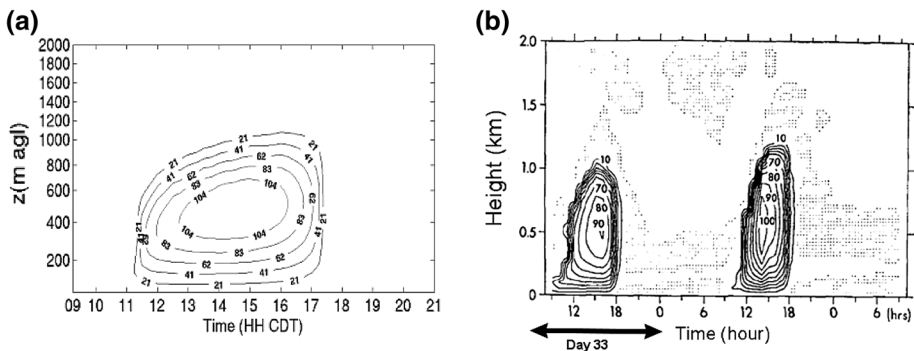


Fig. 9 Spatial and temporal distribution of momentum eddy diffusivities K_m ($\text{m}^2 \text{ s}^{-1}$) simulated for **a** YSU, and **b** by Yamada and Mellor [26]

concentration field, depends on the manner turbulent parameters are related to dynamical and thermodynamic properties and their changes in the PBL. For this reason, it is necessary to parameterize the turbulent transport in a shear dominated stable PBL (near the ground) and the overlying decaying convective turbulent diffusion (associated with RL).

Turbulent dispersion in a shear-dominated stable PBL is generated close to the ground by mechanical processes that are related to wind shear. In the stable PBL there is a competition between wind shear generated turbulence and stabilizing effects of stratification. Therefore, for the description of the dispersion of pollutants in the sunset transition time, here a stable surface layer will be considered, in which a continuous turbulence and a negative turbulent heat flux coexist [68].

The following relationship for longitudinal, lateral, and vertical eddy diffusivities K_i ($i = u, v, w$) derived by Degrazia [69], represents the turbulent diffusion in a shear-dominated stable PBL:

$$K_z = C_z \frac{(1 - \frac{z}{h})^{\frac{3}{2}} u^*}{1 + 3.7 \left(\frac{z}{L(z - \frac{z}{h})^{\frac{3}{2}}} \right)} \tag{2}$$

where $C_z = 0.41$, L is the Obukhov length, u^* is the surface layer friction velocity, z is the altitude above ground level, and h is the height of the stable layer.

According to Garrat [70], the decay of the CBL usually occurs in late afternoon and towards sunset over land under clear skies, when the surface buoyancy flux decreases rapidly towards zero. As a result of the removal of the source for TKE under these conditions, the TKE and other turbulent properties decay in the deep, near-adiabatic remnant of the daytime boundary.

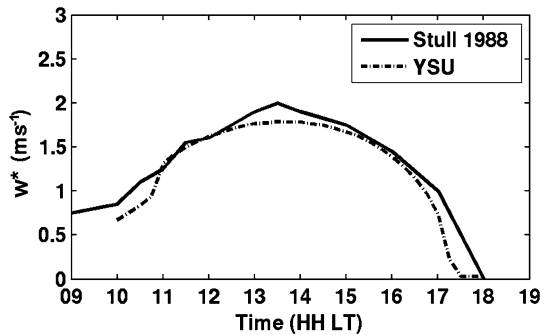
Recently, a general method to derive eddy diffusivities in a decaying turbulence in the daytime CBL has been proposed by Goulart et al. [71]. This method is based upon a model for the budget equation describing the three-dimensional (3D) turbulence energy density spectrum and the Taylor statistical diffusion theory. Therefore, an analytical solution for the budget equation is obtained in terms of an initial 3D spectrum, which describes the observed turbulent spectrum in the daytime CBL. Furthermore, as a consequence of the non-isotropic decaying convective turbulence, this initial 3D spectrum is calculated from a 1D spectrum by the use of a complex mathematical methodology developed by Kristensen et al. [72]. The following relationships proposed by Goulart et al. [71] represent good fits to the decaying convective eddy diffusivities calculated from the theoretical model described above:

$$\frac{K_z}{w^* Z_i} = \frac{0.079}{\sqrt{1 + 2 \times t^* \text{ }^{1.7}}} \tag{3}$$

$$t^* = \frac{t \times w^*}{Z_i} \tag{4}$$

where z_i is the height of the mixing layer, w^* is the velocity scale, and t is time from the beginning of the decay. The eddy diffusivities given by Eq. (3) were compared with those generated from LES data for a decaying CBL [65]. Note that close to the end of the afternoon the surface heat flux begins to weaken as a result of the decreasing sun’s elevation. Consequently, the convective velocity scale w^* (Fig. 10) decreases and z_i remains constant. The great advantage of using this equation is the fact that this formula is

Fig. 10 Convective velocity scale w^* calculated by the YSU PBL scheme and presented in Stull [1]



computationally faster than the numerical integrations in the theoretical model. As a consequence, this algebraic formulation for the eddy diffusivities can be useful for the solution of large and complex atmospheric diffusion models.

We tested a modification of the YSU scheme, applying both Eqs. (2) and (3) suggested by Carvalho et al. [24] for the case when the simulation did not present positive surface fluxes, i.e. at around 17:00 LT and the results from the simulation were compared with the results of the standard YSU scheme (Fig. 11). Overall, the results show visible differences in the calculation of the momentum eddy diffusivity K_m for the transition period. While the standard version of YSU quickly shows values less than $10 \text{ m}^2 \text{ s}^{-1}$ after 17:00 LT (Fig. 11a) the modified version shows a more gradual reduction of K_m , from 17:30 LT to 19:00 LT, with K_m decreasing from 20 to $<10 \text{ m}^2 \text{ s}^{-1}$ during this time period (Fig. 11b). The YSU standard scheme calculated similar values for the convective velocity scale w^* compared to Stull [1] (Fig. 10). The gradual reduction of K_m with time in the modified YSU seems to represent more realistically the decrease of turbulence intensity of the convective mixed layer than the standard YSU. The convective decay condition allows some continuous turbulence in the RL in the early evening, which is not present in the standard model. Figure 11c presents the difference between the standard and the modified YSU scheme for the first 3 lowermost levels of SCM from 17 to 21 LT, which refers to the start of development of SBL. The modified YSU calculated a less mixed SBL than the standard YSU with a difference of up to $0.2 \text{ m}^2 \text{ s}^{-1}$.

To assess how the modifications of eddy diffusivity calculation impacted the results of the YSU PBL parameterization for the evening transition, we analyzed the spatial and temporal variation of the state variables air temperature, wind speed and specific humidity for the transition period until 21 LT (Fig. 12a–c, respectively). The small change in K_m between the standard and the modified YSU scheme resulted in changes in the state variables, albeit not enough to present a significant improvement in the model. The higher

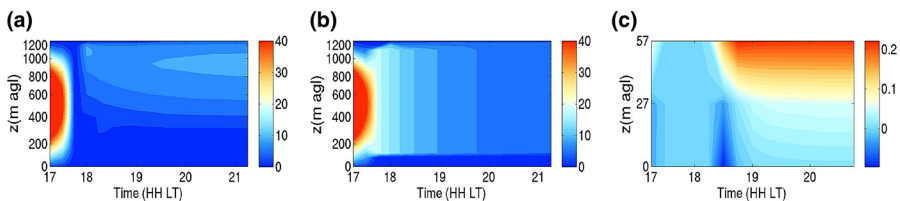


Fig. 11 Spatial and temporal distribution of momentum eddy diffusivities ($\text{m}^2 \text{ s}^{-1}$) for **a** the standard, **b** the modified YSU, and **c** the difference between standard and the modified YSU

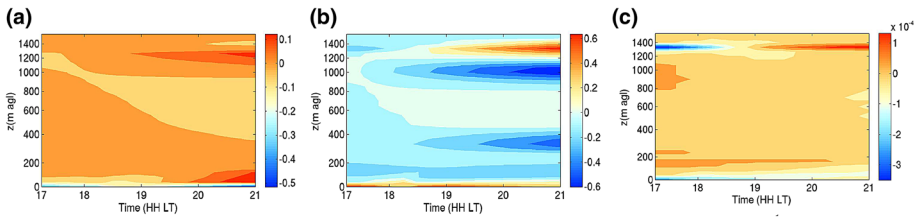


Fig. 12 Calculated spatial and temporal differences for **a** air temperature (K), **b** wind speed and (m s^{-1}) **c** specific humidity (g kg^{-1}) for the modified YSU

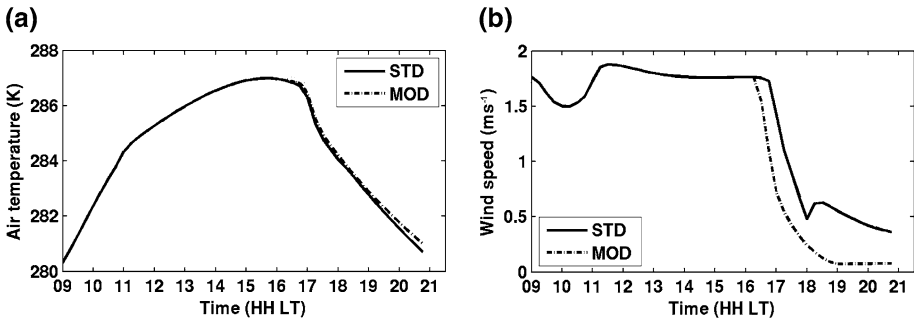


Fig. 13 Calculated **a** air temperature (K) at 2 m above ground, and **b** wind speed (m s^{-1}) at 10 m above ground for the standard (STD) and modified (MOD) YSU

differences were observed near the surface. The changes in the state variables were up to 0.1 K , 0.6 m s^{-1} , and 0.003 g kg^{-1} for air temperature, wind speed and specific humidity, respectively.

Most of the problems in meteorological and air quality models are associated with the representation of the nighttime period, which depends on the evening transition characterization. Many biases related to surface temperature, wind, and pollutants related to these periods are reported in the literature (e.g. [73–75]). Some authors reported a systematically warm bias and an overestimation of wind speeds close to the surface during nighttime, suggesting that strong coupling between the SBL and RL in the PBL scheme would increase these biases [76, 77]. To analyze possible improvements of the suggested modification (i.e. a set of eddy diffusivity equations representing the transition characteristics of a sunset period with a SBL below and a CBL decaying turbulence aloft), model results for air temperature at 2 m and the wind speed at 10 m above the ground are presented in Fig. 13a, b, respectively. Compared with the standard YSU scheme, the modified YSU exhibits a little higher values for the 2 m air temperature (up to 0.1 K around 21 LT). However, the 10 m wind speed is significantly impacted by less mixing in the SBL. The wind speed decreases faster in the modified YSU compared to the standard YSU scheme and presents lower values after the sunset. These values were up to 0.5 m s^{-1} lower than in the standard YSU scheme.

4 Conclusions

In this study, the evening transition of the well known day 33 of the Wangara experiment has been investigated using an idealized Weather and Research Forecasting (WRF version 3.6) simulation at different scales. The results of Large Eddy Simulation (LES) within the

Single-Column Model (SCM) provide insights about current divergences between simulation and observation. We studied a 12-h period between 09–12 LT on August 16, 1967, focusing on the simulation of vertical mixing especially during the transition between daytime and nighttime.

In summary, the sensitivity analysis conducted with both LES and SCM showed that all the simulations are in reasonable agreement with the observations, the discrepancies between the model and the observations become larger during and after the sunset PBL, and the model captures reasonably well the rapid decrease of vertical mixing during the evening transition.

The LES reflected the typical diurnal characteristics of the PBL, ranging from nearly-neutral, convective, to stable conditions during the entire simulation. Both LES simulations captured reasonably well the transition of the CBL to a SBL. However, some difference occur between LES-HM and LES-YSU, e.g. with regard to vertical variations of TKE and its temporal changes. This differences are most probably due to different surface fluxes intensities.

We implemented a modification in the eddy diffusivities equation in the YSU PBL scheme, which took into account an alternative parameterization for the SBL and a parameterization for the convective decay regime typically observed in the RL. However, this modification did not lead to noticeable changes in the state variables during the evening transition.

The integrated approach combining observational data with supplementary information provided from LES were useful to assess the performance of WRF in simulating the PBL evening transition. As mentioned by Lothon et al. [61] the evening transition displays complex characteristics, which are difficult to observe and model due to turbulence intermittency and anisotropy, horizontal heterogeneity, and rapid changes in time. Thus, there are still open questions about the dynamic and turbulence structure of this period, and this complexity imposes extra challenge for numerical simulation. Operational air quality forecast models such as the Weather Research and Forecast with Chemistry (WRF/Chem), the Community Multi-scale Air Quality Model (CMAQ), and the Comprehensive Air Quality Model with Extensions (CAMx) are usually run at a horizontal resolution ranging from 1 to 100 km and the output concentration fields have a temporal resolution of up to 1 h frequency. These spatial and temporal resolutions are at the limit of the present model capacity and are not yet sufficient to completely represent the fast changes in the state variables. Most of these restrictions are related with too coarse initial conditions.

This work applied a parameterization based on the current knowledge of convective decay of the PBL and in particular included for the first time the description of the decay of turbulence characteristics of the RL in a well used NWP. Further tests with different meteorological conditions need to be performed to fully explore the benefit of the proposed parameterization, for instance addressing different intensities of stratification. Our work goes beyond the work of Carvalho et al. [24], who describe the importance of the decaying convective turbulence in a PBL in the dispersion of pollutants during the sunset period, as we studied an appropriate set of eddy diffusion equations which are not only suitable for NWP but also computationally inexpensive.

With expected further increase of model resolution in space and in time, the evening transition period needs to be further explored, in particular with respect to the vertical diffusion and mixing of pollutants, which will be important to improve the performance of AQMs (e.g. WRF/Chem, CMAQ, CAMx, etc.).

Acknowledgements We acknowledge the financial support provided by Coordination for the Improvement of Higher Education Personnel (CAPES). Anna Fitch at NCAR is acknowledged for providing updated WRF LES packages for WRF version 3.6.

References

1. Stull RB (1988) An introduction to boundary layer meteorology. Kluwer, Dordrecht
2. Caughey SJ, Wyngaard JC, Kaimal JC (1979) Turbulence in the evolving stable boundary layer. *J Atmos Sci* 36:1041–1052
3. Grant ALM (1997) An observational study of the evening transition boundary-layer. *Q J R Meteorol Soc* 123:657–677
4. Beare RJ, Edwards JM, Lapworth AJ (2006) Simulation of the observed evening transition and nocturnal boundary layers: large-eddy simulation. *Q J R Meteorol Soc* 132:81–99
5. Mahrt L (1981) The early evening boundary layer transition. *Q J R Meteorol Soc* 107:329–343
6. Taylor GI (1917) The formation of fog and mist. *Q J R Meteorol Soc* 43:241–268
7. Richardson LF (1920) The supply of energy from and to atmospheric eddies. *Proc R Soc Lond A* 97:354–373
8. Acevedo OC, Fitzjarrald DR (2001) The Early Evening Surface-Layer Transition: temporal and Spatial Variability. *J Atmos Sci* 58:2650–2667
9. Grimsdell AW, Angevine WM (2002) Observations of the afternoon transition of the convective boundary layer. *J Appl Meteorol* 41:3–11
10. Brazel AJ, Fernando HJS, Hurt JCR, Selover N, Hedquist BC, Pardyjak E (2005) Evening transition observations in Phoenix, Arizona. *J Appl Meteorol* 44:99–112
11. Edwards JM, Beare RJ, Lapworth AJ (2006) Simulation of the observed evening transition and nocturnal boundary layers: single-column modelling. *Q J R Meteorol Soc* 132:61–80
12. Sastre M, Yague C, Roman CC, Maqueda G, Salamanca F, Viana S (2012) Evening transitions of the atmospheric boundary layers: characterization case studies and WRF simulations. *Adv Sci Res* 8:39–44. doi:10.5194/asr-8-39-2012
13. Kosovic B, Curry JAA (2000) large eddy simulation study of a quasi-steady stably stratified atmospheric boundary layer. *J Atmos Sci* 57:1052–1068
14. Beare RJ, MacVean MK, Holtslag AAM, Cuxart J, Esau I, Golaz J-C, Jimenez MA, Khairoutdinov M, Kosovic B, Lewellen D, Lund TS, Lundquist JK, McCabe A, Moene AF, Noh Y, Raasch S, Sullivan PP (2006) An intercomparison of large-eddy simulations of the stable boundary layer. *Bound Layer Meteorol* 118:247–272
15. Noh Y, Cheon WG, Hong S-Y, Raasch S (2003) Improvement of the K-profile model for the planetary boundary layer based on large eddy simulation data. *Bound Layer Meteorol* 107:401–427
16. Troen I, Mahrt L (1986) A simple model of the atmospheric boundary layer: sensitivity to surface evaporation. *Bound Layer Meteorol* 37:129–148
17. Sharan M, Gopalakrishnan SG (1997) Comparative evaluation of eddy exchange coefficients for strong and weak wind stable boundary layer modeling. *J Appl Meteorol* 36:545–559
18. Cuxart J, Holtslag AAM, Beare RJ, Bazile E, Beljaars ACM, Cheng A, Conangla L, Ek MB, Freedman F, Hamdi R, Kerstein A, Kitagawa H, Lenderink G, Lewellen D, Maillhot J, Mauritsen T, Perov V, Schayes G, Steeneveld G-J, Svensson G, Taylor P, Weng W, Wunsch S, Xu K-M (2006) Single-column model intercomparison for a stably stratified atmospheric boundary layer. *Bound Layer Meteorol* 118:273–303
19. Steeneveld GJ, van de Wiel BJH, Holtslag AAM (2006) Modeling the evolution of the atmospheric boundary layer coupled to the land surface for three contrasting nights in CASES-99. *J Atmos Sci* 63:920–935
20. Mauritsen T, Svensson G, Zilitinkevich SS, Esau I, Enger L, Grisogono B (2007) A total turbulent energy closure model for neutrally and stably stratified atmospheric boundary layers. *J Atmos Sci* 64:4113–4126
21. Baas P, Bosveld FC, Lenderink G, van Meijgaard E, Holtslag AAM (2010) How to design single-column model experiments for comparison with observed nocturnal low-level jets. *Q J R Meteorol Soc* 136:671–684
22. Kumar V, Svensson G, Holtslag AAM, Meneveau C, Parlange MB (2010) Impact of surface flux formulations and geostrophic forcing on large-eddy simulations of diurnal atmospheric boundary layer flow. *J Appl Meteorol Climatol* 49:1496–1516. doi:10.1175/2010JAMC2145.1

23. Bosveld FC, Baas P, Steeneveld G-J, Holtslag AAM, Angevine WM, Bazile E, Bruijn E, Deacu D, Edwards J, Ek M, Larson V, Pleim J, Raschendorfer M, Svensson G (2014) The third GABLS inter-comparison case for evaluation studies of boundary-layer models. Part B: results and process understanding. *Bound Layer Meteorol* 152:157–187. doi:[10.1007/s10546-014-9919-1](https://doi.org/10.1007/s10546-014-9919-1)
24. Carvalho JC, Degrazia GA, Domenico A, Goulart AG, Cuchiara GC, Mortarini L (2010) Simulating the characteristic patterns of the dispersion during sunset PBL. *Atmos Res* 98:274–284. doi:[10.1016/j.atmosres.2010.06.009](https://doi.org/10.1016/j.atmosres.2010.06.009)
25. Clarke RH, Dyer AJ, Brook RR, Reid DG, Troup AJ (1971) The Wangara experiment: boundary layer data. *Div Meteorol Phys Tech* 19:362
26. Yamada T, Mellor G (1975) A simulation of the Wangara atmospheric boundary layer data. *J Atmos Sci* 32:2309–2329
27. André JC, Moor G, Lacarrere P, Therry G, Vachot R (1978) Modeling the 24-hour evolution of the mean and turbulent structure of the planetary boundary layer. *J Atmos Sci* 35:1861–1883
28. Musson-Genon L (1995) Comparison of different simple turbulence closures with a one-dimensional boundary layer model. *Mon Weather Rev* 123:163–180
29. Hacker JP, Rostkier-Edelstein D (2007) PBL state estimation with surface observations—a column model, and an ensemble filter. *Mon Weather Rev* 135:2958–2972. doi:[10.1175/MWR3443.1](https://doi.org/10.1175/MWR3443.1)
30. Skamarock WC, Klemp JB, Dudhia J, Gill DO, Barker DM, Duda MG, Huang H-Y, Wang W, Powers JG (2008) A description of the Advanced Research WRF version 3. NCAR Technical Note NCAR/TN-475STR. 113
31. McNider RT, Pielke RA (1981) Diurnal boundary-layer development over sloping terrain. *J Atmos Sci* 38:2198–2212
32. Hong SY, Dudhia J, Chen SH (2004) A revised approach to ice microphysical processes for the bulk parameterization of clouds and precipitation. *Mon Weather Rev* 132:103–120
33. Mlawer EJ, Taubman SJ, Brown PD, Iacono MJ, Clough S (1997) Radiative transfer for inhomogeneous atmospheres: RRTM, a validated correlated-k model for the longwave. *J Geophys Res* 102:16663–16682
34. Dudhia J (1989) Numerical study of convection observed during the Winter Monsoon Experiment using a mesoscale two-dimensional model. *J Atmos Sci* 46:3077–3107
35. Tewari M, Chen F, Wang W, Dudhia J, LeMone MA, Mitchell K, Ek M, Gayno G, Wegiel GJ, Cuenca RH (2004) Implementation and verification of the unified NOAA land surface model in the WRF model. In: 20th conference on weather analysis and forecasting/16th conference on numerical weather prediction, pp 11–15
36. Paulson CA (1970) The mathematical representation of wind speed and temperature profiles in the unstable atmospheric surface layer. *J Appl Meteorol* 9:857–861
37. Dyer AJ, Hicks BB (1970) Flux-gradient relationships in the constant flux layer. *Q J R Meteorol Soc* 96:715–721
38. Webb EK (1970) Profile relationships: the log-linear range, and extension to strong stability. *Q J R Meteorol Soc* 96:67–90
39. Zhang D-L, Anthes RA (1982) A high-resolution model of the planetary boundary layer—sensitivity tests and comparisons with SESAME-79 data. *J Appl Meteorol* 21:1594–1609
40. Moeng CH, Dudhia J, Klemp J, Sullivan P (2007) Examining two-way grid nesting for large eddy simulation of the PBL using the WRF model. *Mon Weather Rev* 135:2295–2311. doi:[10.1175/MWR3406.1](https://doi.org/10.1175/MWR3406.1)
41. Lenschow DH, Wyngaard JC, Penell WT (1980) Mean field and second-moment budgets in a baroclinic, convective boundary layer. *J Atmos Sci* 37:1313–1326
42. Willis GE, Deardorff JW (1979) Laboratory observations of turbulent penetrative-convection platforms. *J Geophys Res* 84:295–302
43. Schmidt H, Schumann U (1989) Coherent structure of the convective boundary layer derived from large-eddy simulations. *J Fluid Mech* 200:511–562
44. Nieuwstadt FTM, Mason PJ, Moeng CH, Schumann U (1993) Large-eddy simulation of the convective boundary layer: a comparison of four computer codes. In: Durst F et al (eds) *Turbulent shear flows 8*, vol 431. Springer, Berlin, pp 343–367. doi:[10.1007/978-3-642-77674-8_24](https://doi.org/10.1007/978-3-642-77674-8_24)
45. Moeng CH, Sullivan PPA (1994) comparison of shear-and buoyancy-driven planetary boundary layer flows. *J Atmos Sci* 51:999–1022
46. Sullivan PP, McWilliams JC, Moeng C-H (1994) A subgrid-scale model for large-eddy simulation of planetary boundary-layer flows. *Bound Layer Meteorol* 71:247–276. doi:[10.1007/BF00713741](https://doi.org/10.1007/BF00713741)
47. Yamaguchi T, Feingold G (2012) Technical note: large-eddy simulation of cloudy boundary layer with the Advanced Research WRF model. *J Adv Model Earth Syst* 4:M09003. doi:[10.1029/2012MS000164](https://doi.org/10.1029/2012MS000164)

48. Khairoutdinov MF, Randall DA (2003) Cloud resolving modeling of the ARM summer 1997 IOP: model formulation, results, uncertainties, and sensitivities. *J Atmos Sci* 60:607–625. doi:[10.1175/1520-0469\(2003\)060<0607:CRMOTA>2.0.CO;2](https://doi.org/10.1175/1520-0469(2003)060<0607:CRMOTA>2.0.CO;2)
49. Monin AS, Obukhov AM (1954) Basic laws of turbulent mixing in the surface layer of the atmosphere. *Tr AkadNauk SSSR Geofiz* 24:163–187
50. Wyngaard JC, Coté OR (1974) The evolution of a convective planetary boundary layer—a higher-order-closure model study. *Bound Layer Meteorol* 7:289–308. doi:[10.1007/BF00240833](https://doi.org/10.1007/BF00240833)
51. Sun W-Y, Ogura Y (1980) Modeling the evolution of the convective planetary boundary layer. *J Atmos Sci* 37:1558–1572
52. Sun W-Y, Chang C-Z (1986) Diffusion model for a convective layer. Part I: numerical simulation of convective boundary layer. *J Clim Appl Meteorol* 25:1445–1453
53. Xue M, Zong J, Drogemeier KK (1996) Parameterization of PBL turbulence in a multi-scale non-hydrostatic model. In: 11th Conference on numerical weather prediction, Norfolk, VA, American Meteor Society, pp 363–365
54. Hicks BB (1981) An analysis of Wangara micrometeorology: Surface stress, sensible heat, evaporation, and dewfall. NOAA Tech. Memo. ERL ARL-104, NOAA/Air Resources Laboratories, Silver Spring, MD, 36
55. Basu S, Vinuesa J-F, Swift A (2008) Dynamic LES modeling of a diurnal cycle. *J Appl Meteorol Climatol* 47:1156–1174. doi:[10.1175/2007JAMC1677.1](https://doi.org/10.1175/2007JAMC1677.1)
56. Rappenglück B, Perna R, Zhong S, Morris GA (2008) An analysis of the vertical structure of the atmosphere and the upper-level meteorology and their impact on surface ozone levels in Houston/TX. *J Geophys Res* 113:D17315. doi:[10.1029/2007JD009745](https://doi.org/10.1029/2007JD009745)
57. Mahrt L (1999) Stratified atmospheric boundary layers. *Bound-Layer Meteor* 90:375–396. doi:[10.1023/A:1001765727956](https://doi.org/10.1023/A:1001765727956)
58. Darbieu C, Lohou F, Lothon M, Vilà-Guerau de Arellano J, Couvreur F, Durand P, Pino D, Patton EG, Nilsson E, Blay-Carreras E, Gioli B (2015) Turbulence vertical structure of the boundary layer during the late afternoon transition. *Atmos Chem Phys* 15:10071–10086. doi:[10.5194/acp-15-10071-2015](https://doi.org/10.5194/acp-15-10071-2015)
59. Rizza U, Miglietta MM, Degrazia GA, Acevedo OC, Marques EP (2013) Sunset decay of the convective turbulence with large-eddy simulation under realistic conditions. *Phys A* 392:4481–4490. doi:[10.1016/j.physa.2013.05.009](https://doi.org/10.1016/j.physa.2013.05.009)
60. Lothon M, Lohou F, Pino D, Couvreur F, Pardyjak ER, Reuder J, Vilà-Guerau de Arellano J, Durand P, Hartogensis O, Legain D, Augustin P, Gioli B, Lenschow DH, Faloua I, Yagüe C, Alexander DC, Angevine WM, Bargain E, Barrié J, Bazile E, Bezombes Y, Blay-Carreras E, van deBoer A, Boichard JL, Bourdon A, Butet A, Campistron B, de Coster O, Cuxart J, Dabas A, Darbieu C, Deboudt K, Delbarre H, Derrien S, Flament P, Fourmentin M, Garai A, Gibert F, Graf A, Groebner J, Guichard F, Jiménez MA, Jonassen M, van den Kroonenberg A, Magliulo V, Martin S, Martínez D, Mastroiello L, Moene AF, Molinos F, Moulin E, Pietersen HP, Pignatelli B, Pique E, RománCascón C, Rufin-Soler C, Saïd F, Sastre-Marugán M, Seity Y, Steeneveld GJ, Toscano P, Traullé O, Tzanos D, Wacker S, Wildmann N, Zaldei A (2014) The BLLAST field experiment: boundary-Layer Late Afternoon and Sunset Turbulence. *Atmos Chem Phys* 14:10931–10960. doi:[10.5194/acp-14-10931-2014](https://doi.org/10.5194/acp-14-10931-2014)
61. Shaw WJ, Barnard JC (2002) Scales of turbulence decay from observations and direct numerical simulations. In: Proceedings of the 15th symposium on boundary layers and turbulence, 15–19 July 2002, Wageningen
62. Sorbjan Z (1997) Decay of convective turbulence revisited. *Bound Layer Meteorol* 82:503–517. doi:[10.1023/A:1000231524314](https://doi.org/10.1023/A:1000231524314)
63. Nadeau DF, Pardyjak ER, Higgins CW, Fernando HJS, Parlange MB (2011) A simple model for the afternoon and early evening decay of convective turbulence over different land surfaces. *Bound Layer Meteorol* 141:301–324
64. Nieuwstadt FTM, Brost RA (1986) The decay of convective turbulence. *J Atmos Sci* 43:532–546
65. Hong SY, Noh Y, Dudhia J (2006) A new vertical diffusion package with an explicit treatment of entrainment processes. *Mon Weather Rev* 134:2318–2341. doi:[10.1175/MWR3199.1](https://doi.org/10.1175/MWR3199.1)
66. Foken T (2006) 50 years of the Monin–Obukhov similarity theory. *Bound Layer Meteorol* 119:431–447. doi:[10.1007/s10546-006-9048-6](https://doi.org/10.1007/s10546-006-9048-6)
67. Nielsen-Gammon J, Hu X, Zhang F, Pleim J (2010) Evaluation of planetary boundary layer scheme sensitivities for the purpose of parameter estimation. *Mon Weather Rev* 138:3400–3417. doi:[10.1175/2010MWR3292.1](https://doi.org/10.1175/2010MWR3292.1)
68. Nieuwstadt FTM (1984) The turbulent structure of the stable, nocturnal boundary layer. *J Atmos Sci* 41:2202–2216
69. Degrazia GA, Anfossi D, Carvalho JC, Mangia C, Tirabassi T (2000) Turbulence parameterization for PBL dispersion models in all stability conditions. *Atmos Environ* 34:3575–3583

70. Garrat JR (1992) *The Atmospheric Boundary Layer*. Cambridge University Press, Cambridge
71. Goulart AG, Vilhena M, Degrazia G, Flores D (2007) Vertical, Lateral and longitudinal eddy diffusivities for a decaying turbulence in the convective boundary layer. *Ecol Model* 204:516–522. doi:[10.1016/j.ecolmodel.2007.02.004](https://doi.org/10.1016/j.ecolmodel.2007.02.004)
72. Kristensen L, Lenschow D, Kirkegaard P, Courtney M (1989) The spectral velocity tensor for homogeneous boundary layer. *Bound Layer Meteorol* 47:149–193. doi:[10.1007/BF00122327](https://doi.org/10.1007/BF00122327)
73. Miao JF, Chen D, Wyser K, Borne K, Lindgren J, Strandvall MKS, Thorsson S, Achberger C, Almkvist E (2008) Evaluation of MM5 mesoscale model at local scale for air quality applications over the Swedish west coast: influence of PBL and LSM parameterizations. *Meteorol Atmos Phys* 99:77–103. doi:[10.1007/s00703-007-0267-2](https://doi.org/10.1007/s00703-007-0267-2)
74. Hu X-M, Klein PM, Xue M (2013) Evaluation of the updated YSU planetary boundary layer scheme within WRF for wind resource and air quality assessments. *J Geophys Res* 118:10490–10505. doi:[10.1002/jgrd.50823](https://doi.org/10.1002/jgrd.50823)
75. Wang C, Jin S (2014) Error features and their possible causes in simulated low-level winds by WRF at a wind farm. *Wind Energy* 17:1315–1325. doi:[10.1002/we.1635](https://doi.org/10.1002/we.1635)
76. Zhang H, Pu Z, Zhang X (2013) Examination of errors in near-surface temperature and wind from WRF numerical simulations in regions of complex terrain. *Weather Forecast* 28:893–914. doi:[10.1175/WAF-D-12-00109.1](https://doi.org/10.1175/WAF-D-12-00109.1)
77. Ngan F, Kim H, Lee P, Al-Wali K, Dornblaser B (2013) A study of nocturnal surface wind speed overprediction by the WRF-ARW model in Southeastern Texas. *J Appl Meteorol Climatol* 52:2638–2653. doi:[10.1175/JAMC-D-13-060.1](https://doi.org/10.1175/JAMC-D-13-060.1)